Inland Water Mapping Based on GA-LinkNet From CyGNSS Data

Qingyun Yan, *Member, IEEE*, Yuhan Chen, Shuanggen Jin, *Senior Member, IEEE*, Shuci Liu, Yan Jia, *Member, IEEE*, Yinqing Zhen, Tiexi Chen, and Weimin Huang, *Senior Member, IEEE*

***Abstract*— The sensitivity of Cyclone Global Navigation Satellite System (CyGNSS) data to inland water bodies was well documented, however, its advantage over other sensors has seldom been reported. In this work, a semantic segmentation method is adopted for detecting inland water bodies using the CyGNSS data. The widely used LinkNet with the global attention mechanism (GAM) and atrous spatial pyramid pooling (ASPP), namely GA-LinkNet, is equipped to better extract water distributions. The performance comparison with an existing method and other deep networks proved the accuracy and effectiveness of this approach. Satisfactory agreement between the derived and referenced water masks was achieved, with the overall accuracy being 0.959 and 0.976, the mean intersection over union being 0.785 and 0.641, and the F1 scores being 0.879 and 0.781 for the Amazon and Congo regions, respectively. Furthermore, underestimation of water by the reference data was shown during evaluation, which proves the usefulness of the CyGNSS-derived water mask for improving the existing water mask products.**

***Index Terms*— Cyclone Global Navigation Satellite System (CyGNSS), Global Navigation Satellite System-Reflectometry (GNSS-R), inland water mapping, LinkNet, soil moisture (SM).**

I. Introduction

IT IS well known that inland water is a critical part in offering water resources for lives and supporting various human activities, for example, agricultural and industrial processes [1]. As such, it is of utter importance to fully understand the spatio-temporal distribution and variability of inland water bodies. Remote-sensing (RS) techniques have emerged as an excellent tool to fulfill this task. Several water mask datasets derived based on optical sensors, for example, the global surface water (GSW) product [2], are with fine spatial resolutions. However, the presence of clouds and dense vegetation disable effective observations and make surface water undetectable from optical images. In contrast, microwave signals at some frequency bands can provide all-day/-weather surveillance even for regions under canopies due to their good penetration capability [3]. Passive radiometry data are usually with low spatial resolutions (25–50 km) that may not be sufficient for small-scale water body monitoring. Active sensors, such as synthetic aperture radar (SAR), have satisfactory spatial resolutions but the instrumental cost is generally high, limiting the size of constellations and consequently resulting in long revisit times.

State-of-the-art semantic segmentation methods have recently demonstrated superb capability in water body classification from SAR and optical images [12], [13]. Various networks have been tested, and most of them produced satisfactory results despite slight differences in accuracy. Although semantic segmentation has been applied to versatile RS scenes with various data, to the authors' best knowledge, its application with Cyclone Global Navigation Satellite System (CyGNSS) data has not been conducted. This work aims at achieving accurate inland water classification by integrating both GNSS-R and semantic segmentation techniques, with whose validation a new perspective of CyGNSS-based RS is raised. Furthermore, the superiority of CyGNSS in capturing water body presence over other sensors is demonstrated, offering a valid and necessary complement to existing water mask products. It should be noted that the design and modification to semantic segmentation algorithms can be arbitrary and to find the "optimal" network for the best accuracy is impractical. Thus, exhausting/listing a bunch of networks and making intercomparison among them are beyond the current work's focus. Nonetheless, endeavors have been made in testing popular frameworks, and the exciting results are to be compactly presented. The rest of this letter is organized as follows. The CyGNSS and reference water mask data are detailed in Section II. The design of deep networks for CyGNSS-based inland water mapping is presented in Section III. Experiments, evaluation, and discussions are provided in Section IV. Conclusions are summarized in Section V.

Manuscript received 25 September 2022; revised 14 November 2022; accepted 6 December 2022. Date of publication 8 December 2022; date of current version 3 February 2023. The work of Qingyun Yan was supported in part by the Key Laboratory of Land Satellite Remote Sensing Application, Ministry of Natural Resources of the People's Republic of China, under Grant KLSMNR-G202206; and in part by the National Natural Science Foundation of China under Grant 42001362. *(Corresponding author: Tiexi Chen.)*

Qingyun Yan, Yuhan Chen, and Yinqing Zhen are with the Key Laboratory of Meteorological Disaster, Ministry of Education (KLME)/Joint International Research Laboratory of Climate and Environment Change (ILCEC)/Collaborative Innovation Center on Forecast and Evaluation of Meteorological Disasters (CIC-FEMD), Nanjing University of Information Science and Technology (NUIST), Nanjing 210044, China.

Shuanggen Jin is with the School of Remote Sensing and Geomatics Engineering, Nanjing University of Information Science and Technology (NUIST), Nanjing 210044, China, also with the School of Surveying and Land Information Engineering, Henan Polytechnic University, Jiaozuo 454000, China, and also with the Shanghai Astronomical Observatory, Chinese Academy of Sciences, Shanghai 200030, China.

Shuci Liu and Tiexi Chen are with the School of Geographical Sciences, Nanjing University of Information Science and Technology (NUIST), Nanjing 210044, China (e-mail: txchen@nuist.edu.cn).

Yan Jia is with the Department of Surveying and Geoinformatics, Nanjing University of Posts and Telecommunications, Nanjing 210023, China.

Weimin Huang is with the Faculty of Engineering and Applied Science, Memorial University, St. John's, NL A1B 3X5, Canada.

Digital Object Identifier 10.1109/LGRS.2022.3227596

1558-0571 © 2022 IEEE. Personal use is permitted, but republication/redistribution requires IEEE permission.
See https://www.ieee.org/publications/rights/index.html for more information.

Authorized licensed use limited to: Henan Polytechnic University. Downloaded on February 03,2023 at 09:45:13 UTC from IEEE Xplore. Restrictions apply.

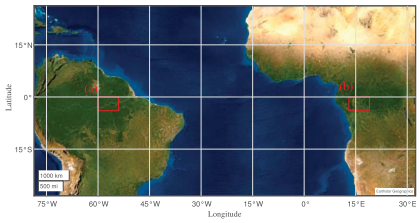

Fig. 1. Study areas of (a) Amazon and (b) Congo rivers (red boxes).

II. Datasets

Parts of the Amazon and Congo rivers spanning over [4°S, 0°N][53°W, 59°W] and [4°S, 0°N][13°W, 19°W] are, respectively, selected and are marked by red boxes in Fig. 1(a). The detailed procedures for preparing CyGNSS RS data along with the reference water masks are described as follows.

A. CyGNSS Data

The CyGNSS Level 1 version 3.0 datasets collected in 2019 and 2020 are used in this work (available at https://podaac-tools.jpl.nasa.gov/drive/files/allData/cygnss/L1/v3.0). The CyGNSS data provide bistatic measurements that are acquired from eight spacecraft. For each payload, four observations can be obtained per second (per 0.5 s after July 2019) and every measurement represents the average during its sampling interval. Specular points (SPs) travel on Earth at a speed of 6 km/s, thus the along-track resolution is about 6 km (3 km for data starting from July 2019). The spatial resolution of each measurement varies with the viewing geometry and the roughness near/at SP. When the surface is relatively flat, the received signal is deemed to be coherent and mainly from the Fresnel zone whose size is about 0.5 km [10]. As such, assuming that the CyGNSS data are dominated by coherent components, its spatial resolution can be regarded as 0.5 × 6 km or 0.5 × 3 km up to the sampling rate. Differing from previous works [9], [10], [11] that aggregate data merely using the recorded SP, this work takes along-track samplings into account to better represent the data acquisition process (see a similar procedure by 14). In addition, a spatial resolution of 500 m is set in this work for gridding CyGNSS data and they are annually batched (with a temporal resolution of one year). However, the temporal resolution can be improved to weekly, monthly, or seasonal scales with the sacrifice of spatial resolution (also noted in [9]).

B. Reference Water Mask

Two datasets providing water masks are employed as reference water masks here, specifically, the global surface water (GSW) data [2] and the WorldCover 2020 v100 product (available online at https://viewer.esa-worldcover.org/worldcover/). The yearly classification data for the years 2019 and 2020 from the GSW data [2] are employed, which consist of labels for land, permanent, and seasonal water. In this work, the latter two labels are grouped as "water," together with the label of land, forming a binary classification task. The spatial resolution of GSW data is 30 m. One 500 × 500 m grid (the spatial resolution considered in this work) will be assigned as "water" as long as it includes one or more 30 × 30 m water pixels. Such threshold is determined based on visual inspection that is also affirmed by the sensitivity of CyGNSS data to fractional water presence [3]. Given the fact that the GSW data are based on optical sensors, its accuracy in dense-canopy-covered regions can be demised [10]. Thus, the WorldCover 2020 v100 data, which are of a spatial resolution of 10 m and are derived based on the Sentinel-2 data as well as the Sentinel-1 microwave backscattering measurements, are selected as a complement to GSW data. The labels of permanent water bodies and herbaceous wetlands are treated as "water" here. Downsampling such label data into a 500-m-grid follows the same strategy as the one stated above. The water masks reproduced from both the GSW and WorldCover 2020 are combined to represent the reference data, and more specifically, a 500-m grid is regarded as "water" when either of these two data is labeled as water [see Fig. 2(a) and (b)].

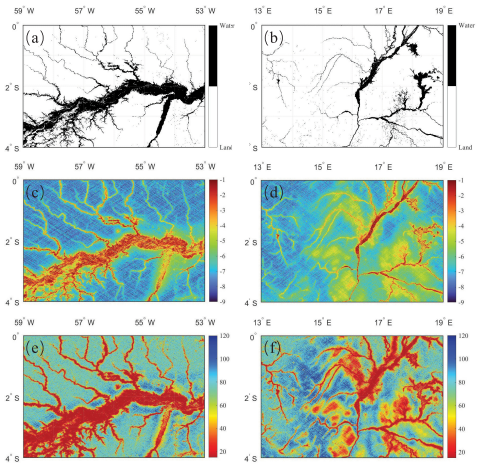

Fig. 2. (a) and (b) Water masks, (c) and (d) CyGNSS SR in log-scale, and (e) and (f) observable of Amazon and Congo rivers for the year 2020, the left and right panels are for Amazon and Congo, respectively.

III. Inland Water Classification Method

Here, the proposed approach for extracting inland water bodies from CyGNSS data is presented, consisting of deriving CyGNSS measurements and constructing a LinkNet-based model.

A. Calculation of CyGNSS Observables

Assuming dominated by the coherent part, the CyGNSS surface reflectivity (SR, Γ) can be calculated as [4], [5], [8]

$$\Gamma = \frac{\sigma (R_t + R_r)^2}{4\pi (R_t R_r)^2} \tag{1}$$

where σ is the bistatic radar cross section, and R_t and R_r are the distances from SP to the transmitter and the receiver respectively, which are accessible in the above-mentioned CyGNSS L1 dataset. In addition to SR, an indicator of CyGNSS delay-Doppler map (DDM)'s spread (pixel number

Authorized licensed use limited to: Henan Polytechnic University. Downloaded on February 03,2023 at 09:45:13 UTC from IEEE Xplore. Restrictions apply.

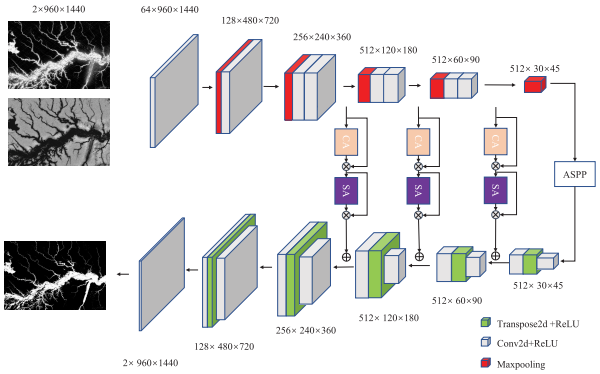

Fig. 3. Structure of the designed GA-LinkNet, where ReLU is rectified linear units.

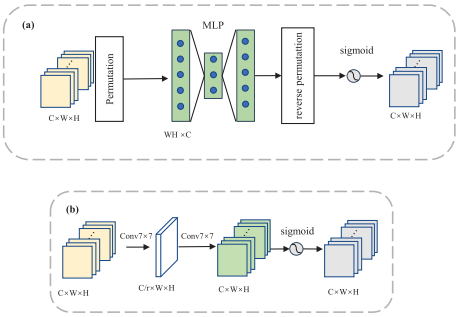

Fig. 4. Block diagrams of GAM. (a) Channel attention (where MLP stands for multilayer perception). (b) Spatial attention.

observable, hereafter, observable) that depicts surface roughness [15] is employed as well. Both CyGNSS data for the study area are shown in Fig. 2.

B. Construction of Semantic Segmentation Networks

LinkNet [16] is a widely used semantic segmentation architecture that can achieve a pixelwise classification task. The water distribution in an image is complicated. Some water paths can spread over the full image, some can be thin or small, while some lakes can be large, and intersections are always present. To effectively extract the complex distribution of inland water bodies, the global attention mechanism (GAM) [17] and atrous spatial pyramid pooling (ASPP) [18] are integrated into LinkNet in this work, and hereafter, the designed LinkNet is referred to as GA-LinkNet. GA-LinkNet contains the encoder, GAM, ASPP, and decoder modules, and its framework is shown in Fig. 3, for which the upper and lower brackets represent the encoder and decoder parts, respectively.

Inputs to GA-Link consist of CyGNSS SR and observable, and the size is 960×1440. Instead of ResNet18 that is adopted in the original Linknet, VGG11 is selected as an encoder here and its better performance will be shown later in Section IV-B. To reduce information loss and acquire more detailed features, GAM is integrated into the network through skip connections [16] between the last three blocks of the encoder and the decoder. GAM contains two submodules of channel attention (CA) and spatial attention (SA) (see Fig. 4 for illustration and more details can be found in [16]). ASPP involves a series of dilated convolution blocks that can enlarge the field of view and obtain multiscale context information. In this work, ASPP is attached to the ends of the encoder and the decoder, and its structure follows that in [18]. For a general introduction to semantic segmentation networks, one can refer to [19].

IV. Experiments and Evaluation

A. Network Training

Here, the proposed GA-LinkNet-based inland water mapping is performed and evaluated. Data collected in 2020 over both Amazon and Congo rivers were employed as the training set since the associated water masks were based on both GSW and WorldCover data that better-revealed water underneath dense vegetation. For CyGNSS SR and observable, their annual medians were utilized at each grid to mitigate the track-wise noise in original data [20].

The number of maximum training epochs was set as 800 and the learning rate was set as 3e-4. Moreover, the learning rate would decrease by half when the total loss stopped decreasing over three consecutive epochs, and the training would be terminated if the total loss ceased to reduce during five continuous epochs. In addition, the Adam optimizer [21] was deployed as the network optimizer.

B. Overall Test Results

In the subsequent classification phase, the data from 2019 were first accumulated and the median of each grid cell was selected to produce a new prediction. The estimations were tested with the GSW 2019 water mask with/without combining WorldCover 2020. Due to a lack of historical data from the WorldCover dataset, the 2020 version was used here. Through the first stage of assessment, the performance of various selected methods was compared, specifically, U-Net, LinkNet (ResNet18), and the proposed GA-LinkNet (along with its associated ablation experiments) were operated. In addition, the RUSBoost method [11] was also included in the appraisal because it outperformed an earlier work [10]. The performance indexes considered here included the overall accuracy (OA), the mean intersection over union (mIoU), and F1 score, which can be calculated through

$$\mathrm{OA} = \frac{\mathrm{TP}+\mathrm{TN}}{\mathrm{TP}+\mathrm{TN}+\mathrm{FP}+\mathrm{FN}} \tag{2}$$

$$\mathrm{mIoU} = \frac{\mathrm{TP}}{\mathrm{TP}+\mathrm{FP}+\mathrm{FN}} \tag{3}$$

$$\mathrm{F1} = \frac{2 \times \mathrm{Precision} \times \mathrm{Recall}}{\mathrm{Precision}+\mathrm{Recall}} \tag{4}$$

$$\mathrm{Precision} = \frac{\mathrm{TP}}{\mathrm{TP}+\mathrm{FP}} \tag{5}$$

$$\mathrm{Recall} = \frac{\mathrm{TP}}{\mathrm{TP}+\mathrm{FN}} \tag{6}$$

where T/F indicates true/false and P/N represents positive/negative. The test results judged by both sets of references are summarized in Table I. The evaluation metrics listed in Table I also demonstrated that the accuracy of semantic

Authorized licensed use limited to: Henan Polytechnic University. Downloaded on February 03,2023 at 09:45:13 UTC from IEEE Xplore. Restrictions apply.

TABLE I
OA, MIOU, AND F1 SCORE OF THE RUSBOOST, LINKNET, U-NET, AND MODIFIED LINKNET

	Amazon						Congo					
	GSW 2019			GSW 2019+ WorldCover2020			GSW 2019			GSW 2019+ WorldCover2020		
Method	OA	mIoU	F1	OA	mIoU	F1	OA	mIoU	F1	OA	mIoU	F1
RUSBoost	.905	.606	.754	.910	.628	.772	.934	.387	.558	.938	.453	.624
U-Net	.950	.730	.844	.952	.744	.853	.976	.612	.7590	.971	.604	.753
LinkNet ResNet18	.946	.692	.818	.946	.699	.823	.976	.572	.728	.969	.538	.699
LinkNet VGG11	.953	.749	.856	.956	.768	.869	976	.624	.769	.975	.658	.794
LinkNet VGG11+GAM	.949	.722	.839	.951	.738	.849	.976	.627	.771	.977	.687	.814
LinkNet VGG11+ASPP	.959	.779	.876	.963	.803	.891	.976	.613	.760	.974	.629	.773
LinkNet VGG11+ASPP+GAM	.959	.785	.879	.965	.817	.899	.976	.641	.781	.981	.728	.843

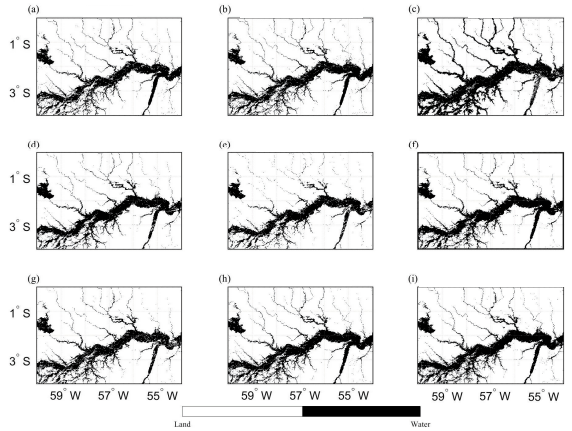

Fig. 5. Water masses for Amazon river using (a) GSW 2019, (b) GSW 2019 + WorldCover 2020, (c) RUSBoost, (d) U-Net, (e) LinkNet (ResNet18), (f) LinkNet (VGG11), (g) LinkNet (VGG11 + GAM), (h) LinkNet (VGG11 + ASPP), and (i) GA-LinkNet (VGG11 + GAM + ASPP).

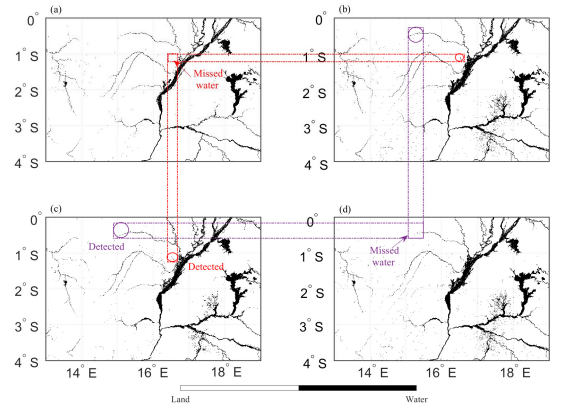

Fig. 6. Water masses for Congo region of (a) GSW, (b) GSW + WorldCover, (c) CyGNSS-based, and (d) WorldCover 2020. Missed detection exists for both GSW and WorldCover datasets.

segmentation-based methods was comparable to each other but distinctly higher than RUSBoost. Notably, the effectiveness and accuracy of the proposed GA-LinkNet were evident by its highest performance among all using either reference dataset. In addition, the overall outputs are displayed in Fig. 5 (for concision, only results for Amazon are presented here), from intuitive inspection of which, the examined methods all successfully generated water masks with similar distribution to the references. The RUSBoost method produced each estimation solely depending on its local information, while the semantic segmentation algorithms utilized the neighboring data (e.g., in the encoding process) to better extract the contextual features of water bodies.

V. CONCLUSION

In this work, a GA-LinkNet is designated for mapping inland water bodies using the CyGNSS L1 data. The network is equipped with GAM and ASPP to better capture water bodies with various shapes and distribution patterns. The performance analyses among RUSBoost, U-Net, LinkNet, and the proposed GA-LinkNet along with its counterparts in ablation tests demonstrated the validity and efficiency of this model. The agreement between the derived and referenced water masks was satisfactory. When compared with GSW 19 (plus WorldCover 2020), the OA was 0.959 (0.965) and 0.976 (0.981), the mIoU was 0.785 (0.817) and 0.641 (0.728), and the F1 scores were 0.879 (0.899) and 0.781 (0.843) for the Amazon and Congo regions, respectively. The results were in better agreement with the combined water masks whose water coverage was higher. Despite the coarsest spatial resolution relative to the other two references, the sensitivity of CyGNSS data to surface water was not compromised. Notably, underestimation of water by GSW and WorldCover was reported and confirmed during evaluation (see Fig. 6), shedding a light on improving the existing GSW and WorldCover products with CyGNSS-derived water mask. Still, it is necessary to compare the results of these methods with in-situ data for validation purposes.

In the future, the water mask reference data involved in training will be further processed and corrected for better agreement and accuracy. In addition, the proposed method will be extended to the CyGNSS's full coverage, producing a pan-tropical inland water distribution map. Moreover, other algorithms that may be better suited for this task will be tested. Furthermore, this study is closely relevant to the European Space Agency (ESA) HydroGNSS mission, an ESA Scout mission under implementation, to be launched in 2024 and the focus of which is global land applications of GNSS-R (with higher spatial coverage than CyGNSS), including wetland/water inundation flag [22]. This work could be applied to the HydroGNSS data for global mapping once they are available. For global application, various influencing factors such as roughness, topography, and biomass will be further considered and other applicable coherence detectors from GNSS-R data should be tested. It should be noted that time

Authorized licensed use limited to: Henan Polytechnic University. Downloaded on February 03,2023 at 09:45:13 UTC from IEEE Xplore. Restrictions apply.

evolution and dynamical aspects are not investigated here, and it is worth studying in the future. Efforts will also be put to detect the extent of flash floods and inundation even under dense vegetation canopy [23], [24].

REFERENCES

[1] S. L. Postel, "Entering an era of water scarcity: The challenges ahead," *Ecol. Appl.*, vol. 10, no. 4, pp. 941–948, 2000.

[2] J.-F. Pekel, A. Cottam, N. Gorelick, and A. S. Belward, "High-resolution mapping of global surface water and its long-term changes," *Nature*, vol. 540, pp. 418–422, Dec. 2016.

[3] C. S. Ruf et al., "A new paradigm in Earth environmental monitoring with the CYGNSS small satellite constellation," *Sci. Rep.*, vol. 8, no. 1, pp. 1–13, Jun. 2018.

[4] C. C. Chew and E. E. Small, "Soil moisture sensing using spaceborne GNSS reflections: Comparison of CYGNSS reflectivity to SMAP soil moisture," *Geosci. Res. Lett.*, vol. 45, no. 9, pp. 4049–4057, May 2018.

[5] Q. Yan, W. Huang, S. Jin, and Y. Jia, "Pan-tropical soil moisture mapping based on a three-layer model from CYGNSS GNSS-R data," *Remote Sens. Environ.*, vol. 247, Sep. 2020, Art. no. 111947.

[6] C. Chew, J. T. Reager, and E. Small, "CYGNSS data map flood inundation during the 2017 Atlantic hurricane season," *Sci. Rep.*, vol. 8, pp. 1–8, Jun. 2018.

[7] P. Ghasemigoudarzi, W. Huang, O. De Silva, Q. Yan, and D. T. Power, "Flash flood detection from CYGNSS data using the RUSBoost algorithm," *IEEE Access*, vol. 8, pp. 171864–171881, 2020.

[8] N. Rodriguez-Alvarez, E. Podest, K. Jensen, and K. C. McDonald, "Classifying inundation in a tropical wetlands complex with GNSS-R," *Remote Sens.*, vol. 11, no. 9, p. 1053, May 2019.

[9] M. Al-Khaldi et al., "Inland water body mapping using CYGNSS coherence detection," *IEEE Trans. Geosci. Remote Sens.*, vol. 59, no. 9, pp. 7385–7394, Sep. 2021.

[10] C. Gerlein-Safdi and C. S. Ruf, "A CYGNSS-based algorithm for the detection of inland waterbodies," *Geophys. Res. Lett.*, vol. 46, no. 21, pp. 12065–12072, Nov. 2019.

[11] P. Ghasemigoudarzi, W. Huang, O. De Silva, Q. Yan, and D. Power, "A machine learning method for inland water detection using CYGNSS data," *IEEE Geosci. Remote Sens. Lett.*, vol. 19, pp. 1–5, 2022.

[12] Z. Dong, G. Wang, S. O. Y. Amankwah, X. Wei, Y. Hu, and A. Feng, "Monitoring the summer flooding in the Poyang lake area of China in 2020 based on Sentinel-1 data and multiple convolutional neural networks," *Int. J. Appl. Earth Observ. Geoinf.*, vol. 102, Oct. 2021, Art. no. 102400.

[13] Z. Miao, K. Fu, H. Sun, X. Sun, and M. Yan, "Automatic water-body segmentation from high-resolution satellite images via deep networks," *IEEE Geosci. Remote Sens. Lett.*, vol. 15, no. 4, pp. 602–606, Apr. 2018.

[14] C. Chew and E. Small, "Description of the UCAR/CU soil moisture product," *Remote Sens.*, vol. 12, no. 10, pp. 1558, May 2020.

[15] Q. Yan and W. Huang, "Spaceborne GNSS-R sea ice detection using delay-Doppler maps: First results from the U.K. TechDemoSat-1 mission," *IEEE J. Sel. Topics Appl. Earth Observ. Remote Sens.*, vol. 9, no. 10, pp. 4795–4801, Oct. 2016.

[16] A. Chaurasia and E. Culurciello, "LinkNet: Exploiting encoder representations for efficient semantic segmentation," in *Proc. IEEE Vis. Commun. Image Process. (VCIP)*, Dec. 2017, pp. 1–4.

[17] Y. Liu, Z. Shao, and N. Hoffmann, "Global attention mechanism: Retain information to enhance channel-spatial interactions," 2021, *arXiv:2112.05561*.

[18] L.-C. Chen, G. Papandreou, I. Kokkinos, K. Murphy, and A. L. Yuille, "DeepLab: Semantic image segmentation with deep convolutional nets, atrous convolution, and fully connected CRFs," *IEEE Trans. Pattern Anal. Mach. Intell.*, vol. 40, no. 4, pp. 834–848, Apr. 2018.

[19] X. Yuan, J. Shi, and L. Gu, "A review of deep learning methods for semantic segmentation of remote sensing imagery," *Expert Syst. Appl.*, vol. 169, May 2021, Art. no. 114417.

[20] Q. Yan et al., "Improving CyGNSS-based land remote sensing: Track-wise data calibration schemes," *Remote Sens.*, vol. 13, no. 14, p. 2844, Jul. 2021.

[21] D. Kingma and J. Ba, "Adam: A method for stochastic optimization," in *Proc. 3rd Int. Conf. Learn. Represent. (ICLR)*, 2015, 2015, pp. 1–15.

[22] M. J. Unwin et al., "An introduction to the HydroGNSS GNSS reflectometry remote sensing mission," *IEEE J. Sel. Topics Appl. Earth Observ. Remote Sens.*, vol. 14, pp. 6987–6999, 2021.

[23] E. Loria et al., "Analysis of scattering characteristics from inland bodies of water observed by CYGNSS," *Remote Sens. Environ.*, vol. 245, pp. 1–16, Apr. 2020.

[24] W. Li et al., "First spaceborne demonstration of BeiDou-3 signals for GNSS reflectometry from CYGNSS constellation," *Chin. J. Environ.*, vol. 34, pp. 1–16, Sep. 2021.

Authorized licensed use limited to: Henan Polytechnic University. Downloaded on February 03,2023 at 09:45:13 UTC from IEEE Xplore. Restrictions apply.